Influence of radiation modelling in under-resolved FDS free-burn simulations

G. Maragkos*, B. Merci

Department of Structural Engineering and Building Materials, Ghent University, Technologiepark-Zwijnaarde 60, 9052 Zwijnaarde, Belgium

Abstract

Focusing on the impact of radiation modelling in under-resolved fire simulations, the paper presents LES of free-burn scenarios. The work aims to evaluate the performance of the current fire modelling capabilities of the Fire Dynamics Simulator (FDS) code and to identify the best practices for FDS practitioners in terms of simulating radiative heat transfer. To this purpose, both optically thin and optically thick approaches are considered and their predictive capabilities over different grid sizes is evaluated. The impact of various radiation modelling parameters with the optically thick approach (i.e., path length, number of solid angles) is also considered. Comparisons of the predicted centerline flame temperatures and axial velocities as well as of the predicted radiative heat fluxes at different locations are presented. Overall, there were obvious differences between the two approaches with the optically thin being more accurate when compared to both experimental data and empirical correlations available in the literature.

Keywords: radiation, heat transfer, free-burn, flame dynamics, FDS

Nomenclature

Abbreviations

CFD Computational Fluid Dynamics

---

*Corresponding author
Email addresses: Georgios.Maragkos@UGent.be (G. Maragkos),
Bart.Merci@UGent.be (B. Merci)

CPU Central Processing Unit

FDS Fire Dynamics Simulator

HRR Heat Release Rate

RTE Radiative Transfer Equation

sgs Sub-Grid Scale

UL Underwriters Laboratories

$WSGG$ Weighted Sum of Gray Gases

English symbols

a Weight factor (-)

A Surface area (m^2)

b Polynomial coefficient (varying units)

c WSGG model coefficient (varying units)

c_p Heat capacity (J/kg/K)

C Correction factor (-)

C_v Deardorff model constant (-)

d WSGG model coefficient $(atm \cdot m)^{-1}$

D Mass diffusivity (m^2/s), diameter (m)

D^* Characteristic fire diameter (m)

E Emission source term (W/m^2)

F Fraction of radiation (-)

g Gravitational acceleration (m/s^2)

G Irradiance (W/m^2)

h_s Sensible enthalpy (J)

I Radiation intensity (W/m^2)

k Kinetic energy (m^2/s^2)

L Path length (m)

L_f Flame height (m)

M_r Molar fraction ratio (-)

N_g Number of gray gases (-)

N_Ω Number of solid angles (-)

p Pressure (Pa, atm)

Pr Prandtl number (-)

$\dot{q}'''$ Heat release rate per unit volume (W/m^3)

$\dot{Q}$ Heat release rate (W)

R Distance (m)

s Stoichiometric oxygen-to-fuel mass ratio (-), direction vector (-)

t Time (s)

T Temperature (K)

u, ν, w Velocity components (m/s)

V Volume (m^3)

Y Mass fraction (-)

z Vertical distance (m)

z_0 Virtual origin (m)

Greek symbols

α Thermal diffusivity (m/s^2)

Δ Filter width (m)

ϵ	Emissivity (-)
θ	Angle (rad)
κ	Absorption coefficient $(\text{m}^{-1}, (\text{atm} \cdot \text{m})^{-1})$
λ	Wavelength (m)
μ	Dynamic viscosity (kg/m/s)
π	Pi number (-)
ρ	Density (kg/m^3)
σ	Stefan - Boltzmann constant $(\text{W}/(\text{m}^2 \cdot \text{K}^4))$
τ	Time scale (s)
χ_r	Radiative fraction (-)
$\dot{\omega}$	Reaction rate $(\text{kg/m}^3/\text{s})$
Ω	Solid angle (sr)

Subscripts / superscripts

∞	Ambient
b	Blackbody
$conv$	Convective
F	Fuel
i	Specie i, gray gas i
j	Order
max	Maximum
min	Minimum
mix	Mixing
n	Radiation band

r Radiation, radiative

ref Reference

t Turbulent

TC Thermocouple

1. Introduction

The study of medium and large-scale fire plumes [1, 2] has received much attention in the past due to the great dangers associated with them (e.g., involving explosions, flame spread). Within this framework, radiation requires special attention as it is typically the dominant mode of heat transfer in many fire scenarios. Due to its importance, the study of radiative heat transfer has received a lot of attention in the literature in the past, both theoretically, experimentally and numerically (e.g., [3, 4, 5, 6, 7, 8, 9, 10, 11]). This is particularly important for accurate prediction of the fuel gasification rate (i.e., either pyrolysis or liquid evaporation) as it is determined by a heat feedback mechanism that strongly depends on radiative heat transfer.

The use of Computational Fluid Dynamics (CFD) has nowadays become an integral part of fire safety engineering which has contributed significantly towards enhancing our understanding of fire-related phenomena and for advancing fire research. CFD-based modelling applied to fire research has made significant progress over the past decades, nevertheless, several challenges still remain and require attention in order to advance predictive fire modelling. Fire research on radiative heat transfer modelling has long been relying on the use of the constant radiative fraction approach. Even though often effective, such an approach is far from predictive as it requires a priori knowledge of the fuel's radiative fraction and can potentially become problematic when multiple fuels, with vastly different radiative fractions, are involved as, e.g., in flame spread scenarios. Additionally, possible issues with the use of the constant radiative fraction approach towards accurately predicting the radiative heat feedback at the fuel surface have to be considered, in particular that there can be an over-estimation of the radiative heat fluxes at the fuel surface [13]. This aspect is mainly attributed to the absence of absorption and/or radiation blockage by fuel vapors and the combustion products close to the fuel surface when this approach is employed. Whether the constant radiative fraction approach is valid for a wide range of scenarios also remains

5

questionable and needs further investigation. For small fires in size (i.e., $D < 1$ m), the local radiative fraction is often approximated to be equal to its global counterpart. However, with increasing fire size, the global value will typically decrease due to a net re-absorption of the thermal radiation by the increasing smoke mantle [14, 15]. The implications from the use of the afore mentioned approach to more complex scenarios (e.g., involving flame spread, compartment fires) remains unknown as fully predictive simulations and direct evaluation of the radiative heat flux components for a wide range of scenarios and fuels is scarce in the literature. Nevertheless, the constant radiative approach also has its advantages. Firstly, it will guarantee that a realistic amount of heat is released for radiation and will be less sensitive than the calculation of the emission term based on the T^4 approach for a wide range of grid sizes (the latter being dependent on the simulation results for temperature). Secondly, the effect of soot radiation can also be (artificially) included, if heavier hydrocarbon fuels are present, by carefully selecting an appropriate value for the radiative fraction without the added complexity of soot modelling, a complex process which is still far from being fully understood. A systematic evaluation of the available radiation models in CFD codes is of great importance in order to gain confidence regarding their accuracy and to avoid compensating errors in the modelling when complex scenarios are considered.

The main objective of the study is to evaluate the performance and predictive capabilities of the CFD code Fire Dynamics Simulator (FDS), when it comes to radiation modelling. The present paper focuses on free-burn scenarios. For evaluation purposes of the CFD simulations, free-burn experiments and well-established empirical correlations and models from the literature are considered. Emphasis is intentionally put on the CFD predictions far away from the fire source (i.e., in the plume region) as the predictions inside the flame are rarely of great interest for fire safety engineers. Rather the radiative heat transfer and flame temperatures far away from the source are the ones that are used for fire safety calculations. Part of the specific objectives is to identify the best modelling options in FDS when it comes to simulating radiative heat transfer scenarios (i.e., from gaseous combustion products). In addition, the work aims to identify some of the best practices for FDS practitioners when it comes to the required spatial resolution in the gas phase solver. The work also aims at addressing several research questions which are all linked to (gas-phase) radiation modelling. Focusing on grid sizes where flames can be under-resolved (i.e., often used for engineering-

type of simulations), the paper will examine the required spatial resolution for accurate fire plume and radiative heat transfer modelling. In addition, the FDS simulations aim to investigate whether the radiative fractions, χ_r, are well predicted with the different modelling approaches, whether the predicted radiative fractions are (strongly) grid-sensitive and whether an under-prediction of χ_r can affect the resulting flame temperatures. Furthermore, it will be investigated whether the choice of path length (related to radiation absorption by a medium) can have a significant effect on the numerical predictions. The influence of the number of solid angles in the prediction of the radiative heat fluxes will also be investigated.

2. Numerical modelling

FDS, developed by NIST, is a low-Mach number, second order accurate, finite difference code with explicit time integration. FDS version 6.7.7 has been used for performing the Large Eddy Simulations (LES) presented in the paper. The code solves the Navier-Stokes equations along with transport equations for species mass fractions and sensible enthalpy. A sensitivity study on different options for modelling radiation is carried out in the context of what most fire engineers (and many fire scientists) do, namely using the default FDS approaches with respect to turbulence (i.e., Deardorff model) and combustion (i.e., EDC). Soot modelling is neglected since the considered fuel (i.e., natural gas) in all the scenarios is only weakly sooty. More details regarding the default options of FDS can be found in [16, 17], hence, only a brief overview is included below.

2.1. Turbulence modelling

Turbulence is modelled using a modified Deardorff model [18] which calculates the sub-grid scale viscosity, μ_{sgs}, as:

$$\mu_{sgs} = \overline{\rho} C_v \Delta \sqrt{k_{sgs}} \tag{1}$$

where $C_v = 0.1$ [19] is a model constant.

The sub-grid scale kinetic energy, k_{sgs}, is calculated from an algebraic relationship, based on scale similarity, as:

$$k_{sgs} = \frac{1}{2}((\overline{u} - \hat{\overline{u}})^2 + (\overline{\nu} - \hat{\overline{\nu}})^2 + (\overline{w} - \hat{\overline{w}})^2) \tag{2}$$

7

where $\overline{u}$ is the LES filtered velocity at length scale Δ and $\hat{\overline{u}}$ is a weighted average of u over the adjacent cells (i.e., test-filtered at length scale 2Δ). The terms $\overline{\nu}$, $\hat{\overline{\nu}}$, $\overline{w}$, $\hat{\overline{w}}$ are defined similarly [17].

2.2. Combustion modelling

The combustion model considers a one-step, infinitely fast, irreversible chemical reaction combined with the eddy dissipation model (EDM) [20] (called 'EDC' in the FDS documentation) for modelling turbulence-chemistry interactions. The EDM model calculates the fuel reaction rate as:

$$\overline{\dot{\omega}'''_F} = -\overline{\rho}\frac{\min(\widetilde{Y}_F, \widetilde{Y}_{O_2}/s)}{\tau_{mix}} \tag{3}$$

where $\widetilde{Y}_F$ and $\widetilde{Y}_{O_2}$ are the fuel and oxygen mass fractions, respectively and s is the stoichiometric oxygen-to-fuel mass ratio.

The mixing time scale, τ_{mix}, is calculated by comparing the mixing times for diffusion (i.e., τ_d), sub-grid scale advection (i.e., τ_u), and buoyant acceleration (i.e., τ_g) as [21]:

$$\tau_{mix} = \min(\tau_d, \tau_u, \tau_g) \tag{4}$$

with

$$\tau_d = \frac{\Delta^2}{D_F}, \quad \tau_u = \frac{C_u\Delta}{\sqrt{(2/3)k_{sgs}}}, \quad \tau_g = \sqrt{\frac{2\Delta}{g}} \tag{5}$$

where D_F is the diffusivity of the fuel, and $C_u = 0.4$ [36] is a model constant calibrated to match Heskestad's flame height correlation [22]. The buoyant time scale is based on a constant acceleration and is expected to control mixing when using coarse grids.

2.3. Radiation modelling

The radiation intensity is considered to be a function of spatial location and angular direction and is obtained by solving the radiative transfer equation (RTE) based on the finite volume method. The RTE for an absorbing, emitting, and non-scattering medium can be written as [23]:

$$\underbrace{s \cdot \nabla I_\lambda}_{\text{Rate of change}} = \underbrace{E}_{\text{Emission source term}} - \underbrace{\kappa I_\lambda}_{\text{Energy loss by absorption}} \tag{6}$$

8

where s is the direction vector, I_λ is the radiation intensity at wavelength λ, E is the emission source term and κ is the local absorption coefficient.

In most numerical simulations of fire scenarios, the spectral dependency of thermal radiation cannot be solved accurately and, in addition, it is very computationally expensive to do so. Instead, the radiation spectrum is typically divided into a number of bands with a separate RTE solved for each band. Under these considerations, a simplified form of the RTE is obtained:

$$s \cdot \nabla I_n = E_n - \kappa_n I_n, \qquad n = 1...N \tag{7}$$

where I_n is the radiation intensity integrated over band n, κ_n is the mean absorption coefficient for that band and N is the total number of bands.

2.3.1. Emission source term

The emission source term for a given band n can be written as:

$$E_n = \kappa_n I_{b,n} \tag{8}$$

where $I_{b,n}$ is the fraction of the blackbody radiation at temperature $\widetilde{T}$:

$$I_{b,n}(x) = F_n \frac{\sigma \widetilde{T}^4}{\pi} \tag{9}$$

expressed using Stefan-Boltzmann law (i.e., $E_b = \sigma \widetilde{T}^4$) and the factor F_n calculated based on the lower (λ_{min}) and upper (λ_{max}) wavelength bounds of a particular band [23].

In the case where the gray gas assumption is not strictly applicable, FDS considers six bands ($N = 6$) for describing the radiation bands of the fuel, CO_2 and H_2O. In such scenarios, the consideration of a gray gas assumption (i.e., $N = 1$) tends to lead to an over-prediction of the emitted radiation. For cases where the gray gas assumption is applicable (i.e., soot radiation is dominant), it is possible to consider a gray gas assumption and, hence, limit the number of bands considered to $N = 1$. In such conditions, $F_n = 1$ (i.e., all the fraction of radiation is emitted in this single band) and the emission source term is given by the blackbody radiation intensity:

$$I_b = \frac{E_b}{\pi} = \frac{\sigma \widetilde{T}^4}{\pi} \tag{10}$$

2.3.2. Calculation of absorption coefficients

An overview of the different approaches available within FDS for calculating the absorption coefficient, κ_n, is presented in this section.

- **'Gray gas'**: This is the default approach for LES (named **'Gray'**). Considering an optically-thick flame, the local absorption coefficient, κ_n, of the gas mixture is calculated as the sum of the individual gases' gray or band-mean absorption coefficients, $\kappa_{n,i}$, as:

$$\kappa_n = \sum_i \kappa_{n,i}(\widetilde{Y}_i, \widetilde{T}) \tag{11}$$

  with $\kappa_{n,i}$, being dependent on gas composition and temperature, calculated by a narrow-band model, RADCAL [24]. RADCAL computes the spectral properties of the species participating in radiation at discrete values of the spectrum and temperature, and returns two alternative mean absorption coefficients for each band, n. The first coefficient is a Planck mean coefficient, $\kappa_{n,i,P}(\widetilde{Y}_i, \widetilde{T})$, dependent on the local composition and temperature, while the second coefficient is an effective absorption coefficient, $\kappa_{n,i,e}(\widetilde{Y}_i, \widetilde{T}, L)$, dependent on the local composition, temperature and path length L. For more details regarding the calculation of the two absorption coefficients the reader is referred to [36]. Only one band is considered by default in FDS ($N = 1$) and the local absorption coefficient is calculated by considering the minimum of the Planck mean coefficient and the effective absorption coefficient:

$$\kappa_{n,i} = \min(\kappa_{n,i,P}, \kappa_{n,i,e}) \tag{12}$$

  The default value for the path length in FDS is $L = 0.1$ m. Alternatively, an estimation of the path length can be also be made as $L = 4V/A$ [16] where V is the volume occupied by the fire and A is the encompassing surface area. For pool fire scenarios (i.e., free-burn cases), V and A can be calculated considering a cone-like flame shape with the burner diameter, D, and the flame height, L_f, (calculated using Heskestad's correlation [22]), as lengths of interest. This approach (named **'Gray-newL'**) is also employed for estimating L here.

- **'Weighted Sum of Gray Gases' (WSGG)**: Instead of solving multiple RTEs, the WSGG model [25] approximates the entire absorption

10

spectrum by calculating the local absorption coefficients as a weighted sum of various gray gases, each being a function of gas composition and temperature. The species that are typically considered are H_2O, CO_2 and soot, while other gases are ignored. Both gray and non-gray WSGG formulations have been evaluated in numerical simulations of fire scenarios in the past (e.g., [26, 27, 28]. Only a non-gray WSGG formulation is available in FDS [17], in which the electromagnetic spectrum is divided in a small number of bands n. The local absorption coefficient in each band is constant and calculated with the approach presented below, hence, the subscript n has been removed for clarity.

The total emissivity, ϵ, of a CO_2 and H_2O mixture is calculated as [29]:

$$\epsilon = \sum_{i=0}^{N_g} a_i \left(1 - e^{-\kappa_i p L}\right) \tag{13}$$

where N_g is the number of gray gases, a_i is the weight factor of the i-th gray gas, κ_i is the absorption coefficient of the i gray gas, p is the sum of the partial pressures of all absorbing gases, and L is the path length. In the present case, four gray gases are used ($N_g = 4$), along with a transparent gas ($i = 0$) which represents the spectral windows between the absorption bands.

The weight factors, a_i, are calculated as a polynomial function of temperature as:

$$a_i = \sum_{j=0}^{4} b_{i,j} T_r^j, \quad i > 0 \tag{14}$$

where $T_r = \widetilde{T}/T_{ref}$ is the normalized temperature and $T_{ref} = 1200$ K is the reference temperature [30]. The emissivity weight factor for the transparent gas is calculated from energy conservation as $a_0 = \sum_{i=1}^{N_g} a_i$.

The polynomial coefficients, $b_{i,j}$, of the i-th gray gas of the j-th order are a function of the molar fraction ratio, M_r, and calculated as:

$$b_{i,j} = \sum_{k=0}^{4} c_{i,j,k} M_r^k \tag{15}$$

11

The absorption coefficients for the gray gases, κ_i, are calculated as:

$$\kappa_i = \sum_{k=0}^{4} d_{i,k} M_r^k \tag{16}$$

with the absorption coefficient of the transparent gas set to zero (i.e., $\kappa_0 = 0 \text{ m}^{-1}$).

With the WSGG model, five bands ($N = 5$) are considered with the local absorption coefficient in each band, n, calculated as:

$$\kappa_n = \kappa_i p_{mix} \tag{17}$$

where p_{mix} is the partial pressure of the CO_2 - H_2O mixture.

The WSGG model coefficients (i.e., $c_{i,j,k}$ and $d_{i,k}$), taken from [29], are obtained for different fuels by fitting Eq. (13) to line-by-line (LBL)-based emissivity databases for different pL values.

2.3.3. Radiation contribution to the energy equation

A typical form of the energy equation for the gas phase in the context of LES, using filtered quantities, can be written as:

$$\frac{\partial(\overline{\rho}\widetilde{h}_s)}{\partial t} + \nabla \cdot (\overline{\rho}\widetilde{u}\widetilde{h}_s) = \frac{D\overline{p}}{Dt} + \nabla \cdot \left[\overline{\rho} \left(\alpha + \frac{\nu_{sgs}}{Pr_t} \right) \nabla \widetilde{h}_s \right] - \nabla \cdot \overline{\dot{q}_r''} + \overline{\dot{q}'''} \tag{18}$$

where $\overline{\rho}$ is the density, $\widetilde{h}_s$ is the sensible energy, $\widetilde{u}$ is the velocity, $\overline{p}$ is the pressure, t is time, α is the thermal diffusivity, ν_{sgs} is the sub-grid scale kinematic viscosity, Pr_t is the turbulent Prandtl number, $\overline{\dot{q}_r''}$ is the radiative heat flux vector and $\overline{\dot{q}'''}$ is the heat release rate per unit volume due to combustion (defined in the case of a single-step reaction as the product of the fuel reaction rate and the heat of combustion of the fuel).

Using the gray gas assumption, considering a single band (i.e., $N = 1$), the radiative heat loss term in the energy equation can be calculated as:

$$\nabla \cdot \overline{\dot{q}_r''} = \kappa_n (4\pi I_b - G) \tag{19}$$

where the total radiation intensity (i.e., irradiance) is calculated as:

$$G = \int_{4\pi} I d\Omega \tag{20}$$

2.3.4. Correction in emission source term

In general, the calculation of the emission source term in Eq. (10) requires special attention as it can be highly grid-sensitive due to its dependence on temperature to the fourth power. For this reason, in regions where combustion takes place (i.e., in which $\chi_r \overline{\dot{q}'''} > 10$ kW/m^3), the emission source term is corrected and Eq. (10) then becomes:

$$I_{b,f} = C\frac{\sigma \widetilde{T}^4}{\pi} \tag{21}$$

with the correction factor C calculated as:

$$C = \frac{\sum(\chi_r \overline{\dot{q}'''} + \kappa_n G)V}{\sum(4\kappa_n \sigma \widetilde{T}^4)V} \tag{22}$$

where χ_r is the radiative fraction of the fuel and V is the cell volume.

By combining Equations (19), (21) and (22), the emission term in cells where combustion takes place (i.e., in the 'flame' region) is based on the constant radiative fraction approach, and takes the following form:

$$\nabla \cdot \overline{\dot{q}_r''} = \chi_r \overline{\dot{q}'''} \tag{23}$$

For 'optically-thin' flames, the net effect of emission minus absorption (i.e., right hand side of Eq. (19)) is then solely based on Equation (23) in every cell in the computational domain where combustion takes place and no modelling of the absorption coefficient is required (i.e., **'Thin'** model). This simple approach guarantees that the correct amount of heat will be released due to radiation, which is particularly useful if coarser grids are employed in the simulations and/or sooty fuels are involved, and avoids the necessity of modelling turbulence-radiation interactions (TRI).

An overview of the different radiation modelling approaches that are used in the FDS simulations, together with the required user-input model parameters, is presented in Table 1.

For a detailed overview of the angular discretization treatment in FDS (i.e., determination of the number of zenith and azimuth angles based on prescribed number of solid angles), the reader is referred to [17].

In terms of computational costs, 'Thin' was the fastest model to run in any of the scenarios considered, followed by 'Gray gas' (i.e., +10%) and 'WSGG' (i.e., +271%).

Table 1: Overview of the various radiation modelling options used in the simulations.

Model	Radiative fraction χ_r (-)	Emission correction	Path length L (m)	Approach
Gray gas				
Gray	Predicted	Yes	0.1	Optically-thick
Gray-newL	Predicted	Yes	$L^* = 4V/A$	Optically-thick
Thin	Prescribed	-	-	Optically-thin
WSGG	Predicted	No	-	Optically-thick

*Calculated as 0.286 m, 0.349 m, 0.363 m for the 100 kW, 500 kW and 1000 kW scenarios, respectively.

2.4. Discussion

It should be noted that the approaches for modelling turbulent combustion and radiation considered in the paper are chosen in the context of numerical simulations of practical fire scenarios with affordable computational costs. These models represent extreme simplifications of the complex dynamics of turbulence, mixing, chemical reaction and radiation occurring in fires with flaming combustion. It is acknowledged that far more advanced models have been developed to incorporate detailed chemistry (i.e., allowing for the prediction of intermediate species and for products of incomplete combustion). Likewise, there are far more advanced radiation models that have been applied in numerical simulations of turbulent flames, abandoning assumptions like optically thin simplifications and describing the gaseous radiation much more accurately. However, the computational cost that comes along with such models is also significantly higher and is often considered prohibitive in fire modelling, certainly by fire engineers but also by many fire scientists. In addition, and perhaps even more importantly, the fuel involved in fires is often unknown or poorly characterized, which poses a very severe limitation to the use of these more advanced turbulent combustion and radiation models in practical fire scenarios. This explains why the models as implemented in FDS, which can be considered very 'basic' in research communities that focus on turbulent combustion or radiation, are state-of-the-art in the fire science and engineering community. With respect to radiation, it is also worth noting that in fires often soot is very dominant and while it is already very difficult to predict soot concentrations (even with the advanced turbulent combustion models mentioned below) if the fuel is well-known, it

becomes almost impossible if the fuel is unknown. Hence it is often not recommendable to opt for very advanced gas radiation models in fire simulations. This said, it is considered worthwhile to devote a brief discussion on turbulent combustion and radiation modelling. It is considered worth exploring these, be it as add-on implementations within the FDS software or through the use of other CFD software, but this is considered beyond the current study, which focuses on FDS as it is (and which is therefore relevant for state-of-the-art simulations in fire engineering and science).

2.4.1. Turbulent combustion

As mentioned, there are more advanced turbulent combustion models than what is used in the present paper (and in most of today's fire simulations), with in principle the potential to predict gas compositions and radiation more accurately. A brief summary of some of these models is outlined below, with some comments added:

- (Unsteady) Laminar flamelet models [31]: The model essentially assumes that the gradient along the flame front can be neglected compared to the gradient perpendicular to it. The flame structure is treated as one-dimensional and a turbulent diffusion flame is viewed as a collection of laminar diffusion flamelets, assuming that the conditions in the immediate surroundings of these flamelets are not (strongly) affected by the overall turbulence. The counterflow diffusion flame configuration is a common laminar flame used to represent a flamelet in a turbulent flow. The flamelet equations are expressed in terms of mixture fraction, scalar dissipation rate (SDR) and time. Non-adiabatic conditions can be accounted for by inclusion of radiation (with different levels of complexity, ranging from an enthalpy deficit with a fixed fraction over the entire mixture fraction space up to inclusion of detailed radiation calculations) and a library of counterflow diffusion flames with variable strain rate is constructed, so that the impact of the SDR can be accounted for and the SDR becomes an independent input parameter (on top of mixture fraction and enthalpy defect). The reader is referred to [11] for illustration of the application of unsteady flamelet model in fire scenarios. One important unresolved issue is the fact that state-of-the-art laminar flamelet models, focusing on species and temperature, do not seem to guarantee the conservation of the total heat release rate [12]. As the heat release rate is a quantity of key importance in fire

15

simulations, this is a significant drawback that must be overcome.

- Conditional moment closure (CMC) [32]: The CMC method does not rely on the assumptions as mentioned for the flamelet methods. In principle therefore this methodology can be considered more general. It is an advanced turbulent combustion model that can predict the conditional averages of species mass fractions and temperature or enthalpy, with mixture fraction as independent variable for the conditioning. The CMC model is, thus, in principle able to determine the chemical source terms with detailed chemistry models. This comes at a high computational expense of an additional computational dimension to the modelling problem: the transport equations for the conditional averages are solved over mixture fraction space, which is discretized into a number of bins. Moreover the equations can be very stiff to solve. An important sub-model choice is the assumption of the conditional scalar dissipation rate model, i.e., the value and profile of SDR in mixture fraction space. Radiation effects can then be accounted for as in laminar flamelet models, ranging from including a heat-loss term directly on the conditional average of temperature or sensible enthalpy, up to inclusion of detailed radiation calculations. The reader is referred to [33] for illustration of the application of CMC in fire scenarios. Very similar to what was mentioned for laminar flamelet models, it is not a priori guaranteed to retrieve the total heat release rate in physical space from integration over mixture fraction space [33, 12], presumably because the profile for conditional heat release rate in mixture fraction space is a narrow spike around stoichiometry, which requires high resolution and which makes integration over mixture fraction space with pre-assumed probability density function (PDF) not straightforward. This deserves further research.

- Transported PDF [34]: The transported PDF approach is perhaps the most advanced turbulent combustion model where turbulence - chemistry interaction is taken into account through the use of transport equations of the probability density function (PDF). The major advantage is that the turbulent combustion source terms in the species equations appear in closed form (in the context of LES, the filtered chemical source terms appear in closed form). Radiation effects can also be considered, using either simplified or very advanced modelling

approaches. However, transported PDF methods are computationally very expensive and given the overall uncertainties in fire simulations and the fact that large computational domains and long durations must be covered in a realistic fire scenario, this technique is not expected to become popular in fire engineering simulations. The reader is referred to [35] for an example in fire simulations.

2.4.2. Radiation

It is worth stressing that the work presented here is not intended to serve as a validation study of FDS in benchmark radiation scenarios nor does it aim to compare the state-of-the-art modelling approaches for modelling radiation that are available in the literature. Instead, the work aims to evaluate the current predictive capabilities of FDS and to identify the best modelling options for CFD practitioners when it comes to simulating radiative heat transfer scenarios. With this in mind, modelling of radiative heat transfer was inevitably limited by the approaches currently available in FDS.

It is worth noting that the experimental cases considered for model evaluation involve pool fires in open atmosphere (i.e., free-burn scenarios) where the soot yield is relatively small compared to the yields of CO_2 and H_2O. The flames in such scenarios could, in principle, then be treated as optically thin without the need to calculate absorption by the colder gases. A posteriori analysis along the centerline of the simulated flames presented in the paper (i.e., 100 kW – 1000 kW with Gray-newL), resulted in values of $\kappa L < 1$, further supporting the idea that the optically thin approximation, as opposed to the use of optically thick models, could be sufficient. In addition, it has been reported that the gray gas assumption in FDS (i.e., optically thick flame using a single radiation band) might not be sufficient in such scenarios and that more radiation bands are needed to provide a more accurate representation of the most important radiation bands of the fuel, CO_2, and H_2O [16]. This aspect can then introduce some uncertainties in the use of the optically thick approach in these scenarios. Nevertheless, the optically thick models (Gray, Gray-newL) were still used and evaluated in the paper since they are the default FDS approach when it comes to radiation and essentially the models that fire engineers will use for typical fire simulations regardless of the scenario considered.

Overall, FDS has been validated in numerous fire-related scenarios [36] exhibiting, in most cases, fairly good accuracy. Several FDS studies specifically focusing on radiation modelling have also been reported in the litera-

ture, e.g., [37, 38]), demonstrating that FDS is capable of accurately simulating radiative heat transfer. Nevertheless, the considered radiation modelling approaches also exhibit several limitations that are worth reporting.

The calculation of the path length as $L = 4V/A$, while used widely in the past, has little basis in physical reality since it suggests that local radiative properties depend on global parameters of the problem. The physics of radiation transfer in high temperature gases mandate that the local absorption coefficient is a function only of local thermodynamic properties (i.e., gas composition and temperature). The path length approach originates decades ago when gas emissivities for isothermal (and with some approximation, non-isothermal/non-homogeneous) layers required a path length. Contemporary approaches for modelling gas radiation have reached a level of sophistication and accuracy that doesn't require such approaches.

The WSGG model, in its customary form, is valid only for spatially constant mole fraction ratios. However, general combustion scenarios yield significantly varying mole fraction ratios and poses a limitation of the considered models. Contemporary models are not limited to constant mole fraction ratios [29] while still having acceptable computational cost.

Contemporary global models such as, e.g., the full spectrum correlated k-distribution (FSCK) method [39] and the spectral-line based weighted-sum-of-gray-gases (SLW) model [40], which have been developed and refined in the last two decades, yield accuracy within a few percent of line-by-line benchmark predictions for a small fraction of the computation time. These global models have now matured to the point that they can be competitive with other models (e.g., WSGG) in terms of computational cost.

3. Experiments

Free-burn experiments conducted by the Underwriters Laboratories (UL) [41] are considered for validation purposes of the numerical simulations. A schematic of the experimental setup, along with the position of the instrumentation used, is presented in Figure 1. A square burner, 0.6 m in diameter and 0.1 m in depth, supported on steel legs is used with its surface raised 0.5 m above the floor. The experiments were conducted under a large hood (i.e., see large gray area in Figure 1) equipped with oxygen consumption calorimetry. The fuel source was positioned such that the geometric center of the burner was positioned under the center of the exhaust hood (shown as the grey area in the figure). The fuel involved is natural gas (composition: 92.2%
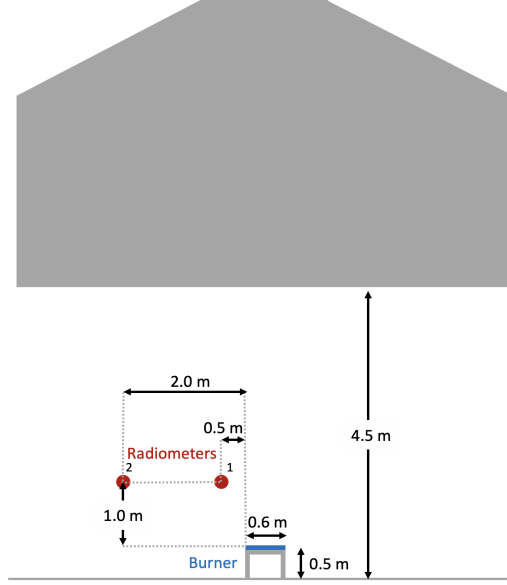
Figure 1: Schematic of the free-burn experiments (side view).

CH_4, 5.8% C_2H_6, 1.3% N_2, 0.7% CO_2) with a calculated heat of combustion of $\Delta H_c = 47784$ kJ/kg. The considered fire sizes are 100 kW, 500 kW and 1000 kW. The measured radiative fraction was reported to be $\chi_r = 0.23$ for all fire sizes [41]. The available experimental data include measurements of radiative heat fluxes through heat flux gauges with an experimental uncertainty of approximately $\pm 8\%$. Additional information about the experiments and the instrumentation can be found in [41].

4. Empirical correlations

Additional validation of the numerical simulations is made by comparison of the CFD predictions to well-established empirical correlations (i.e., focusing on the centerline temperatures and velocities) available in the literature.

Heskestad's correlations for the centerline mean temperature and axial velocity, valid in the plume region, are expressed as [22]:

$$T = \frac{9.1 \left(\frac{T_\infty}{g c_p^2 \rho_\infty^2} \right)^{1/3} \dot{Q}_{conv}^{2/3}}{(z - z_0)^{5/3}} + T_\infty \qquad (24)$$

19

$$U = \frac{3.4 \left(\frac{T_\infty}{c_p T_\infty \rho_\infty} \right)^{1/3} \dot{Q}_{conv}^{1/3}}{(z - z_0)^{1/3}} \tag{25}$$

where T (K) is the mean temperature, T_∞ (K) and ρ_∞ (kg/m³), are the ambient temperature and density, respectively, c_p (J/(kg·K)) is the specific heat at constant pressure, g (m/s²) is the gravitational acceleration, $\dot{Q}_{conv}$ (kW) is the convective heat release rate, U (m/s) is the mean axial velocity and z (m) is the axial distance from the burner surface. In the equations above, the plume region is defined as the axial location, starting from the burner surface, where $z - z_0 > 0.2 \dot{Q}_{conv}^{2/5}$.

The virtual origin, z_0, is calculated as:

$$z_0 = 0.083 \dot{Q}^{2/5} - 1.02D \tag{26}$$

where D is the burner diameter (or effective diameter for non-circular fires). Negative z_0 values, associated with low heat release fires and/or large surface areas, correspond to locations below the actual fuel surface, while positive z_0 values, associated with high heat release rate values and/or small surface areas, correspond to locations above the actual fuel surface.

McCaffrey's correlations for centerline mean temperature and axial velocity, valid in the plume region, are expressed as [1]:

$$T = \frac{\frac{T_\infty}{2g} \left(\frac{1.1}{0.9} \right)^2}{\left(\frac{z}{\dot{Q}^{2/5}} \right)^{5/3}} + T_\infty \tag{27}$$

$$U = \frac{1.1 \dot{Q}^{1/5}}{\left(\frac{z}{\dot{Q}^{2/5}} \right)^{1/3}} \tag{28}$$

where $\dot{Q}$ (kW) is the total heat release rate. In the equations above, the plume region is defined as the axial location, starting from the burner surface, where $z > 0.2 \dot{Q}^{2/5}$. Note that McCaffrey's correlations have been developed based on weak plumes (i.e., 0.3 m square burner for $\dot{Q} = 14.4$ - 57.5 kW).

The point source model [42], presented schematically in Figure 2, considers that the radiative energy is emitted isotropically from a single point source located at mid-height inside a fire and the radiative heat flux can be calculated as:

$$\dot{q}_r'' = \frac{\chi_r \dot{Q} \cos\theta}{4\pi R^2} \tag{29}$$

where χ_r (-) is the radiative fraction of the fuel, $\dot{Q}$ (kW) is the total heat release rate, θ (radians) is the angle between the normal to the target and the line of sight from the target to the point source location, and R (m) is the distance between the point source and the target of interest.
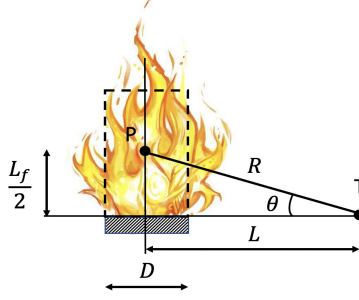

Figure 2: Schematic of the point source model [42].

Beyler [43] suggested that the point source model is mostly accurate for heat fluxes less than 5 kW/m² (i.e., valid for low values of the radiation load). In addition, Fleury [44] found the point source model to be the best performing method, on average, compared to other simplified methods.

5. Numerical setup

A square computational domain with dimensions of 5 m × 5 m × 5 m is used to model the scenarios. The domain is wide enough to freely allow for air entrainment towards the fire plumes and high enough, compared to the flame height of the fire plumes (i.e., $L_f = 3.11$ m based on Heskestad's flame height correlation for the 1000 kW case), so there is no influence of the outlet domain boundary on the fire plume development. The bottom boundary of the computational domain is treated as a wall and represents a floor. All the other boundaries of the computational domain are treated as open, allowing for fresh air to be freely entrained. A rectangular object (i.e., 0.6 cm x 0.6 m and 0.1 m in depth) is used as the burner, with its surface raised 0.5 m above the floor, according to the experimental setup. The top boundary of the object is treated as the surface of the burner with a prescribed mass flow rate to match the experimental HRR based on the reported ΔH_c value of the fuel. The other surfaces of the object are treated as inert walls. The required spatial resolution is an important modelling parameter that requires attention in order to have accurate CFD predictions. An a priori estimation

21

of the required grid size is made by considering values of $D^*/\Delta \geq 15$ (i.e., D^* criterion), which has proven accurate enough for simulations of various fire scenarios with FDS in the past [36]. Based on this, four different uniform grid sizes are considered, i.e., 0.2 m, 0.1 m, 0.05 m and 0.025 m having total number of cells of 16 k, 125 k, 1 mil. and 8 mil., respectively. The resulting grid resolutions of the numerical simulations for each case are presented in terms of D^*/Δ in Table 2. Overall, the a priori criterion of $D^*/\Delta \geq 15$ is met for most of the two finest grid sizes considered (i.e., 0.05 m and 0.025 m), except for the 100 kW scenarios with a grid size of 0.05 m. The ratios of D/Δ would correspond to 3, 6, 12 and 24 for grid sizes of 0.2 m, 0.1 m, 0.05 m and 0.025 m, respectively. In this case, the use of the 'Rule of thumb' (i.e., having at least 10 cells across the burner diameter) also suggests that a grid size of at least 0.05 m should be sufficient for resolving fairly accurately the fire plume dynamics. In addition, the values from Table 2 illustrate that, in general, finer grid sizes are required to accurately simulate smaller fires in terms of HRR. It is worth noting that the 0.2 m grid size is very coarse (i.e., only 3 cells across the burner) and it is not expected to accurately resolve the fire dynamics, hence, not a lot of emphasis will be put in the analysis of these results (i.e., mainly presented as part of a grid sensitivity study). Nevertheless, this grid resolution is used in order to test the predictive capabilities of FDS on such coarse grids (i.e., often used for engineering-type of simulations).

Table 2: Overview of the grid resolutions, in terms of D^*/Δ, for the different scenarios.

$\dot{Q}$ (kW)	D^{*a} (m)	$D^*/0.2$ (-)	$D^*/0.1$ (-)	$D^*/0.05$ (-)	$D^*/0.025$ (-)
100	0.39	1.95	3.9	7.8	15.6
500	0.73	3.65	7.3	14.6	29.2
1000	0.97	4.85	9.7	19.4	38.8

[a]Characteristic fire diameter: $D^* = \left(\frac{\dot{Q}}{\rho_\infty c_p T_\infty \sqrt{g}}\right)^{\frac{2}{5}}$ where $\dot{Q}$ (kW) is the heat release rate of the fire, ρ_∞ (kg/m^3), c_p (kJ/(kg·K)), T_∞ (K) are the density, specific heat and temperature of the ambient air, respectively, while g (m/s^2) is the gravitational acceleration.

The ambient temperature and pressure are set to 15°C and 101325 Pa, respectively. A value of $\chi_r = 0.23$ [41] was prescribed for the radiative

fraction for all scenarios, in accordance with the experiments. The default number of solid angles in FDS ($N_\Omega = 100$) was employed in the simulations, however, a sensitivity study of up to 800 solid angles was conducted for the prediction of the radiative heat fluxes. For comparison to experimental data, a thermocouple (TC) model with diameter $d = 0.0016$ m and the properties of Nickel (i.e., $\epsilon_{TC} = 0.85$, $\rho_{TC} = 8908$ kg/m^3 and $c_{p,\ TC} = 0.44$ kJ/(kg·K)) is used, while for the heat flux gauges, a gauge temperature of 14°C and a gauge emissivity of 0.95 are considered [41].

6. Results

The predictions from the numerical simulations, focusing on different approaches for modelling radiation, are presented in this section. An analysis of the required spatial resolution for accurate fire plume modelling when under-resolved fires are involved (i.e., engineering-type of simulations), is presented. Subsequently, the impact of employing an optically-thick or optically-thin approach is analysed and the influence of using different models for the calculation of the absorption coefficient with the former approach is discussed. In addition, the predicted radiative fractions with the different approaches, along with their impact on the numerical predictions (e.g., flame temperatures), are discussed. Finally, the predicted radiative heat fluxes with the different modelling approaches are assessed and compared to both experimental data and empirical models available in the literature.

6.1. Flame structure

A first qualitative overview of the different scenarios considered in the simulations is depicted in Figure 3, presenting the instantaneous heat release rate per unit volume (i.e., 200 kW/m^3) for different scenarios. The cases considered involve increasing heat release rates from 100 - 1000 kW (bottom to top) and decreasing grid sizes from 0.2 m to 0.025 m (left to right). First of all, it can be seen that the computational domain is high enough to allow for the free development of all fire plumes and also wide enough to allow for air to be freely entrained towards the flame. Overall, there are clearly more turbulent flame structures and clearer puffing (observed in video animations of the simulations) with decreasing grid size for all the cases. In addition, the visual flame heights tend to increase with increasing heat release rate and decreasing grid size.

6.2. Grid sensitivity

Figure 4 presents a grid sensitivity study and reports on the predicted mean and rms centerline temperatures and axial velocities with the 'Gray' model for the different heat release rates considered. The values from Heskestad's [22] and McCaffrey's [1] experimental correlations in the plume region, are presented for comparison purposes. The grid sensitivity study is reported only for the 'Gray' model given, as this is the default model of FDS. Nevertheless, similar findings were obtained with the use of the other models (not included here to avoid repetition).

Even though very coarse, the predictions using the 0.2 m grid size, are able to get the trends correctly and in many cases agree qualitatively with the simulations using finer grid sizes. Some discrepancies are evident (e.g., under-prediction of flame temperatures close to the burner for the 100 kW case and over-prediction of axial velocities in the plume region for all scenarios), however, the predictive capabilities of the simulations even on such
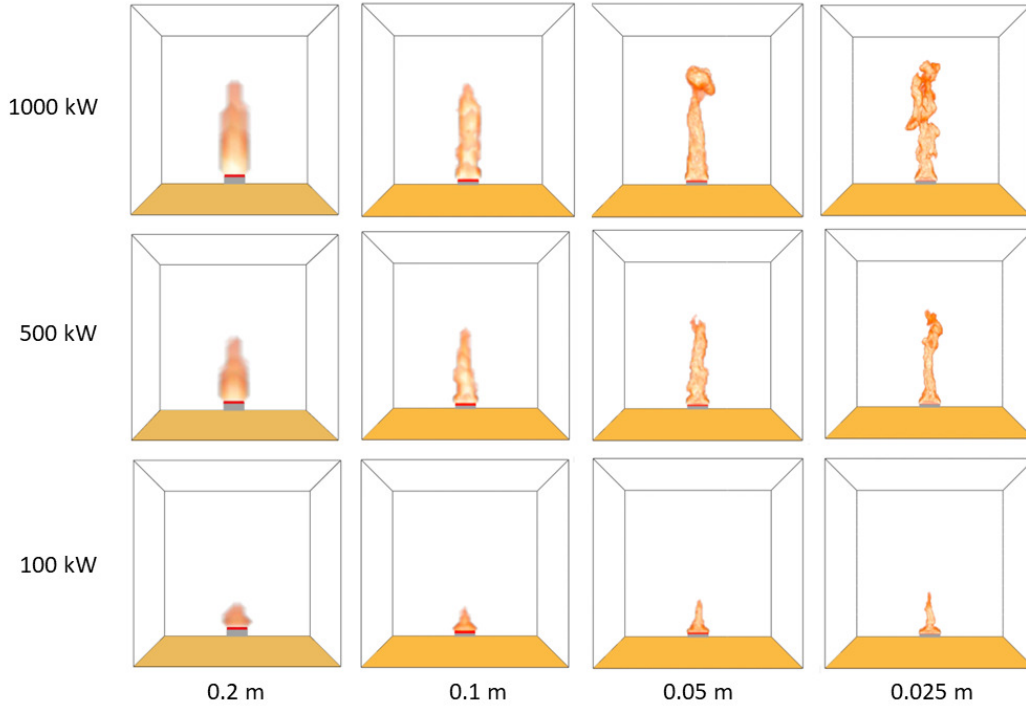
Figure 3: Instantaneous heat release rate per unit volume (200 kW/m^3) for the different scenarios considered with the 'Gray' model.
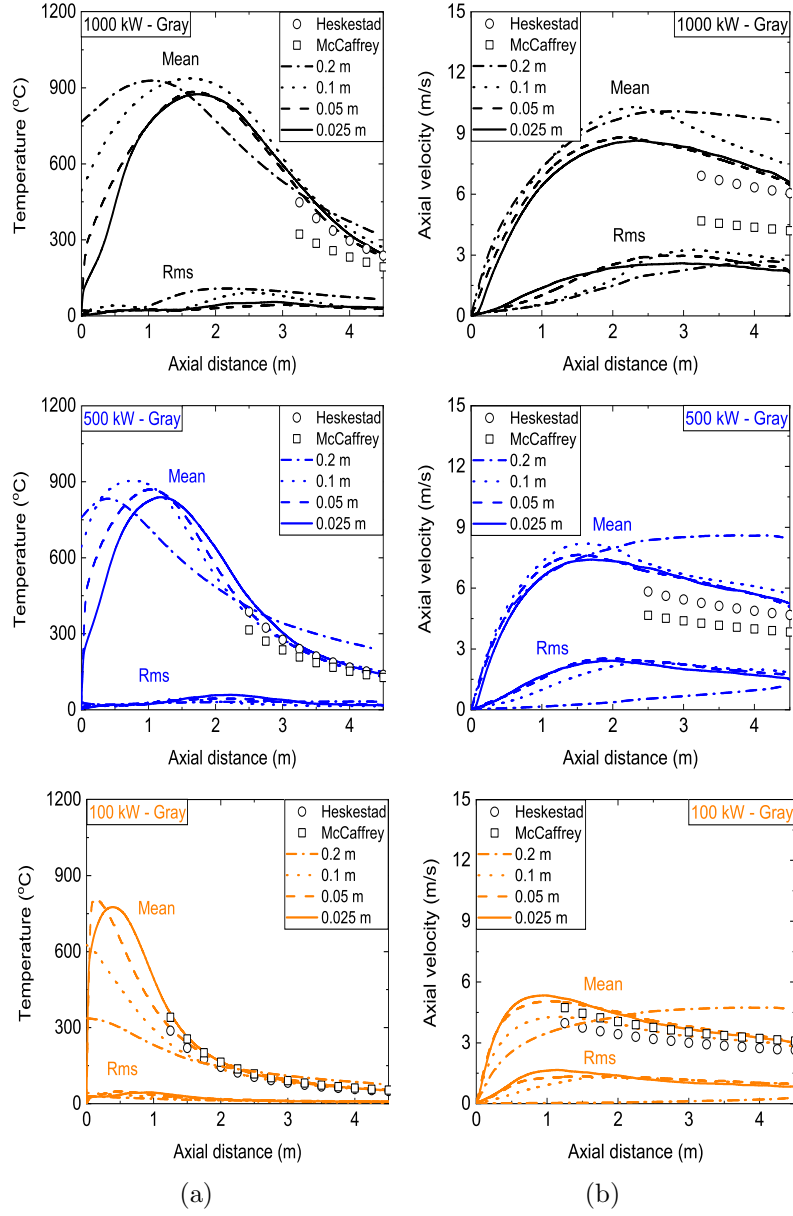
24

Figure 4: Centerline mean and rms (a) temperature and (b) axial velocity with the 'Gray' model for different grid sizes and heat release rates. All symbols refer to mean values (no rms data available).

coarse grids are very encouraging. Overall, there is less grid sensitivity in the predictions between the 0.05 m and 0.025 m grid sizes than when refining the grid size from 0.1 m to 0.05 m. This is to be expected, as finer grid sizes will result in reduced influence from the sub-grid scale (turbulence) modelling. In addition, the maximum flame temperature (on the order of 750 - 900°C depending on the scenario) shifts further downstream with decreasing grid size for all heat release rates, a consequence of the fire plumes developing a fuel rich region above the burner around the centerline as the grid size decreases. The CFD predictions with the finer grid sizes (i.e., 0.05 m, 0.025 m) agree fairly well with the experimental correlations for temperature for all the heat release rates examined. The comparisons for the axial velocity are less favourable, with the numerical simulations slightly over-predicting the values given by Heskestad's correlation. Nevertheless, the comparison to the data from McCaffrey's correlation is reasonable. The presented results indicate that the finer grids employed in the present study (i.e., 0.05 m, 0.025 m) are sufficiently small to capture most of the flow dynamics involved in the cases considered. Overall, the 0.025 m grid size satisfies the various grid resolution criteria for accurate LES (i.e., more than 80% of the turbulent kinetic energy was resolved - results not shown here) and could be considered small enough to accurately simulate the fire plume dynamics in these scenarios. On the other hand, the 0.05 m grid size (and even more so the 0.1 m grid size), can be considered acceptable for engineering-type of simulations while still maintaining a reasonable balance between accuracy and computing cost.

6.3. Radiation model sensitivity

Figures 5 - 6 present the predicted centerline mean temperatures and axial velocities with the different radiation modelling approaches as a function of grid size (i.e., 0.1 - 0.025 m) for different heat release rates. Overall, there are significant differences between the optically-thin (i.e., 'Thin') and optically-thick ('Gray', 'Gray-newL', 'WSGG') approaches and the differences became larger with increasing $\dot{Q}$ for all grid sizes. Even though the largest differences are found on the coarse 0.1 m grid size they are still observable even on the finest grid size employed (i.e., 0.025 m). To explain the differences in the predictions, the predicted radiative fractions from the numerical simulations, χ_r, are analysed and presented in Table 3. The predictions with the 'Thin' model were confirmed to be equal to the prescribed experimental value (i.e., code verification), hence are not presented. Overall, the predictions with the 'Gray' model (i.e., the default approach of FDS for LES) under-predict the

26

experimental values by approximately 11 - 20%, depending on the scenario examined. Decreasing the grid size from 0.1 m to 0.025 m resulted in an increase in the χ_r values by 6 - 10%. The use of another value for the path length (i.e., 'Gray-newL'), compared to the default FDS value of 0.1 m, did not reveal a significant effect in the scenarios examined and only increased the χ_r values by 3 - 6%. The predictions with the 'WSGG' model were not satisfactory and significantly under-predicted the χ_r values by more than 36%. Further investigation of the implementation of the WSGG model in FDS is required (i.e., implicit consideration of a path length in the model, implemented model coefficients, etc.) in order to determine the reasons for the discrepancies observed with this model. The neglect of soot modelling, even if the fuel involved here is only weakly-sooty (i.e., natural gas), and the lack of sufficient grid resolution in the flame region could partially explain the lower radiative fractions for the cases where χ_r is predicted and not pre-scribed or corrected (i.e., in the cases with 'WSGG'). In general, the CFD predictions regarding the centerline mean flame temperatures and axial velocities are in line with the radiative fraction predictions (i.e., under-prediction of χ_r implies smaller amounts of heat being released due to radiation which results in higher flame temperatures and axial velocities) indicating the close relation between the amount of heat being released due to radiation in the simulations and the resulting flow field. The differences between the models (i.e., optically-thin versus optically-thick) become larger with increasing heat release rates for all the grid sizes. In most scenarios, the predictions with the 'Thin' model (i.e., optically-thin approach) are the ones closest to the empirical correlations for the centerline temperature and axial velocity, while the worst predictions are typically the ones obtained with the 'WSGG' model.

6.4. Radiative heat fluxes

Figures 7 - 8 present the predicted radiative heat fluxes at radiometer 1 and 2, respectively, for different radiation modelling approaches, grid sizes and heat release rates with the default number of solid angles in FDS (i.e., 100). The UL experimental data and the predictions using the point source model are also included for validation purposes of the simulations. The CFD predictions close to the burner (i.e., radiometer 1) suggest that the radiative heat fluxes are fairly grid insensitive for $\Delta \leq 0.05$ m. In addition, there is a trend of decreasing heat fluxes with decreasing grid size (i.e., a consequence of the flames being wider and the same amount of heat being distributed on
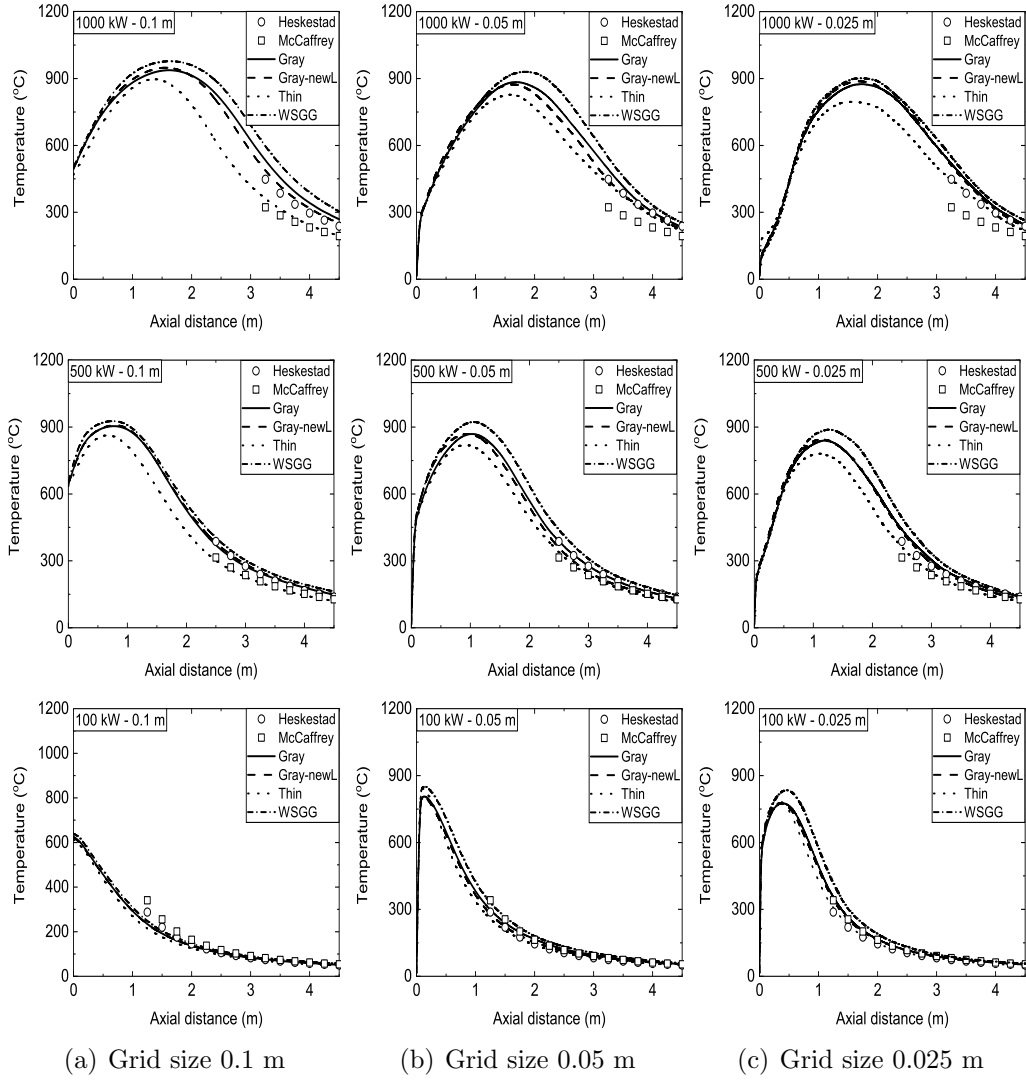
27

(a) Grid size 0.1 m   (b) Grid size 0.05 m   (c) Grid size 0.025 m

Figure 5: Centerline mean temperature as a function of grid size for different heat release rates and different radiation modelling approaches.

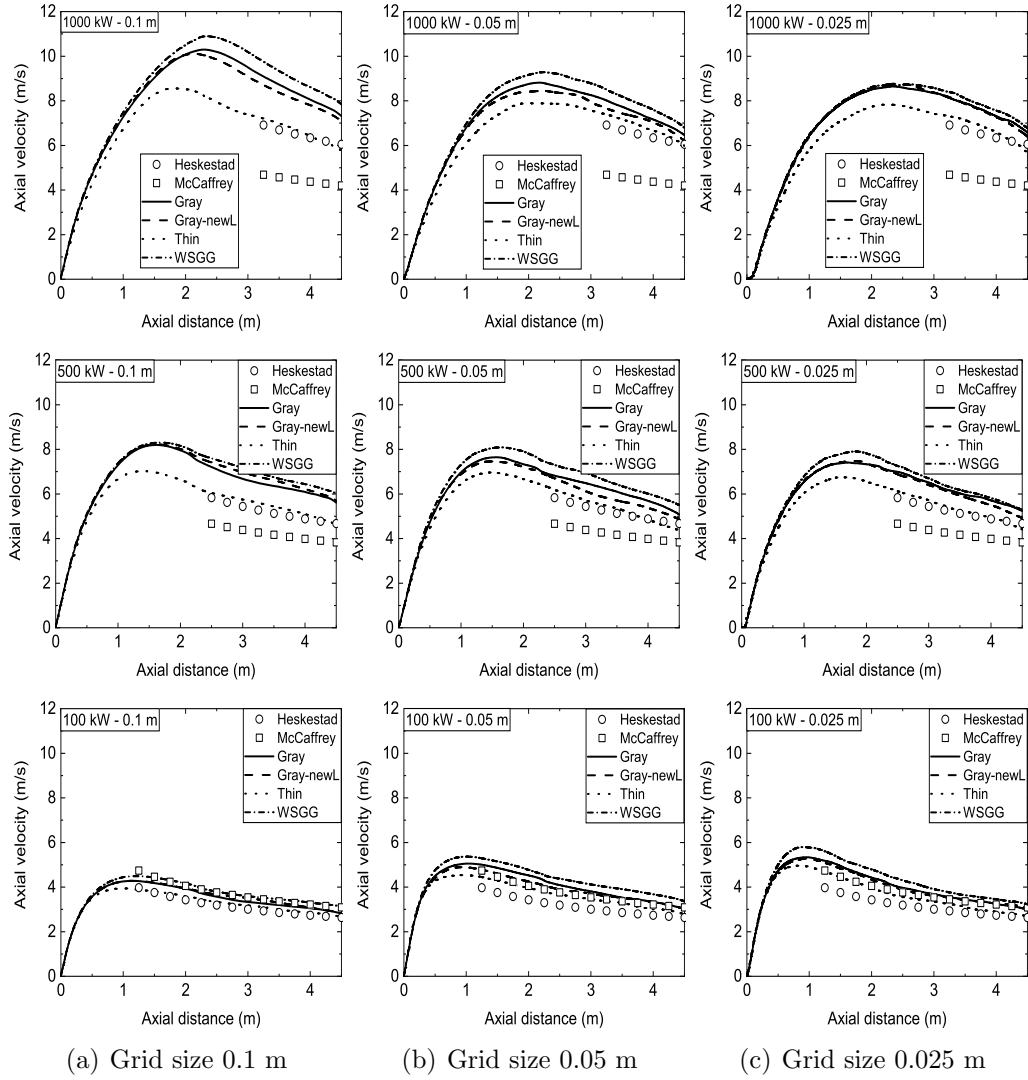(a) Grid size 0.1 m   (b) Grid size 0.05 m   (c) Grid size 0.025 m

Figure 6: Centerline mean axial velocity as a function of grid size for different heat release rates and different radiation modelling approaches.

Table 3: Predicted radiative fractions*, χ_r, using different radiation modelling approaches.

	100 kW	500 kW	1000 kW
Gray			
0.2 m	0.172 (-25%)	0.182 (-21%)	0.183 (-20%)
0.1 m	0.185 (-20%)	0.186 (-19%)	0.184 (-20%)
0.05 m	0.195 (-15%)	0.193 (-16%)	0.189 (-18%)
0.025 m	0.205 (-11%)	0.197 (-14%)	0.196 (-15%)
Gray-newL			
0.2 m	0.181 (-21%)	0.193 (-16%)	0.195 (-15%)
0.1 m	0.193 (-16%)	0.198 (-14%)	0.197 (-14%)
0.05 m	0.202 (-12%)	0.203 (-12%)	0.201 (-13%)
0.025 m	0.211 (-8%)	0.207 (-10%)	0.207 (-10%)
WSGG			
0.2 m	0.103 (-55%)	0.131 (-43%)	0.146 (-36%)
0.1 m	0.127 (-45%)	0.145 (-37%)	0.147 (-36%)
0.05 m	0.147 (-36%)	0.143 (-38%)	0.144 (-37%)
0.025 m	0.146 (-36%)	0.141 (-39%)	0.146 (-36%)
Experiment	0.23	0.23	0.23

*The calculated value with 'Thin' was 0.23 for all scenarios.

fewer cells when the grid is coarser - see Figure 3) with the 'Thin' model predictions being less grid sensitive compared to the other approaches. This can be attributed to the dependence of the emission term in the optically-thick models (i.e., 'Gray', 'Gray-newL' and 'WSGG') on the resolved cell temperature, as opposed to 'Thin', in which the emission term is calculated based on the local heat release rate per unit volume. Overall, there is a general trend of under-predicting the UL experimental data for the radiative heat fluxes in most cases. However, for the lower heat release rate scenario (i.e., 100 kW), the numerical predictions agree fairly well with the point source model. On the other hand, the CFD predictions for the radiative heat fluxes at locations further away from the fire source (i.e., radiometer 2) are, as expected, more sensitive to the spatial and angular discretization. In most cases, there is a general trend of under-predicting the heat fluxes, with the predictions of the 'Thin' model being higher compared to the predictions of the rest of the models. In this case, the CFD predictions agree better with the point source model data for the lower heat release rate (i.e, 100 kW),
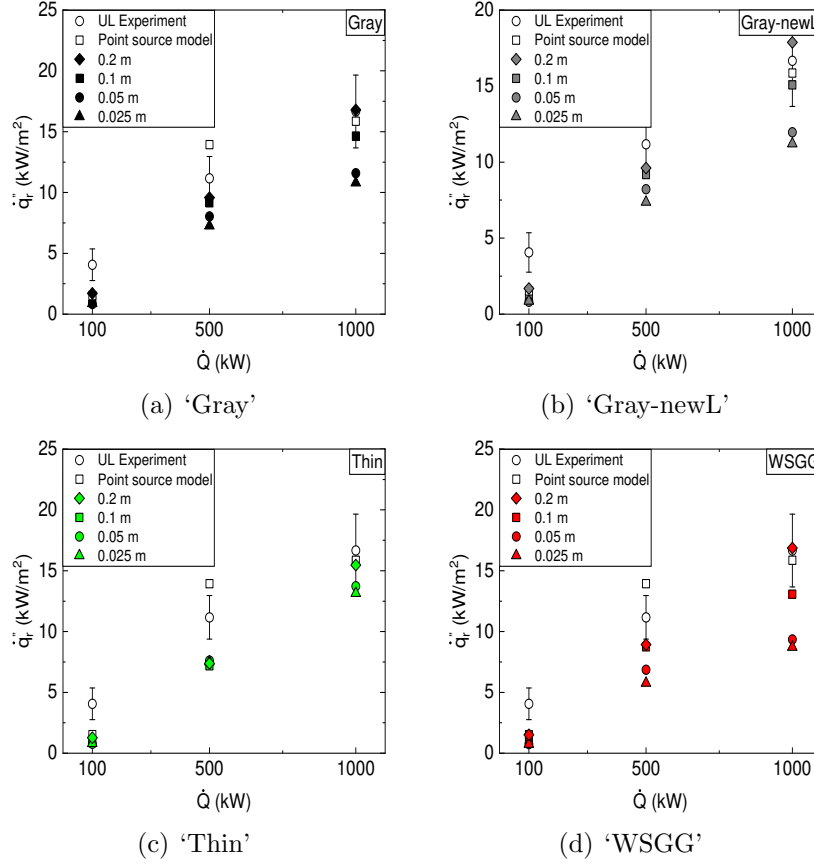
Figure 7: Radiative heat fluxes at radiometer 1 using different radiation modelling approaches with $N_\Omega = 100$.

similarly to what was observed for radiometer 1, and are closer to the UL experimental data for the higher heat release rate case (i.e., 1000 kW).

Figure 9 presents the predicted radiative heat fluxes at two different locations (i.e., radiometers 1 and 2) for different heat release rates and number of solid angles. The sensitivity study is performed with the 0.05 m grid size, previously determined to be accurate enough for simulating these scenarios, and examines the performance of 'Gray-newL' and 'Thin', the two radiation models that performed the best in terms of predicting the flame temperatures and flow field. The UL experimental data and the predicted fluxes with the point source model are also included for validation purposes of the numerical simulations. Overall, the default number of solid angles in FDS (i.e., 100)
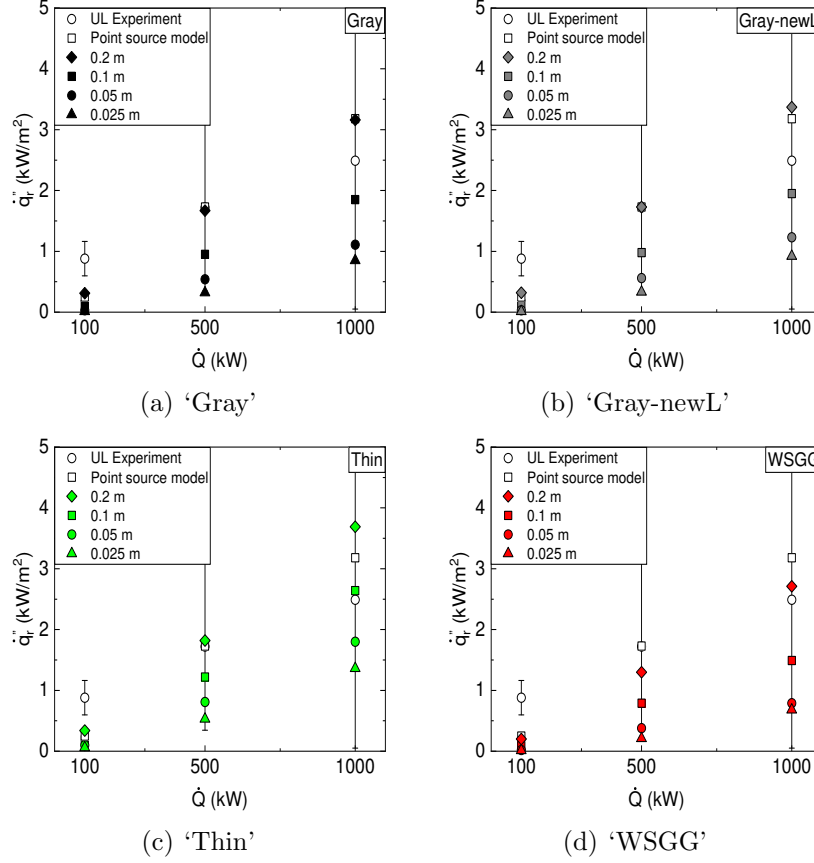
31

Figure 8: Radiative heat fluxes at radiometer 2 using different radiation modelling approaches with $N_\Omega = 100$.

can be considered sufficient for targets that are relatively close to the burner (i.e., radiometer 1) for all the different heat release rates considered. On the other hand, more solid angles (i.e., ≥ 400) are needed for targets positioned far away from the burner (i.e., radiometer 2). In general, there is a fair comparison between the CFD predictions and the experiments / point source model for the higher heat release rate cases (i.e., 500 - 1000 kW). However, the experimental data are significantly higher than both the CFD predictions and the empirical model for the lower heat release case (i.e., 100 kW).

It is worth noting that predicting radiative heat fluxes accurately with the use of simplified / empirical models can be very challenging and inherently includes a lot of uncertainties. The point source model has been reported

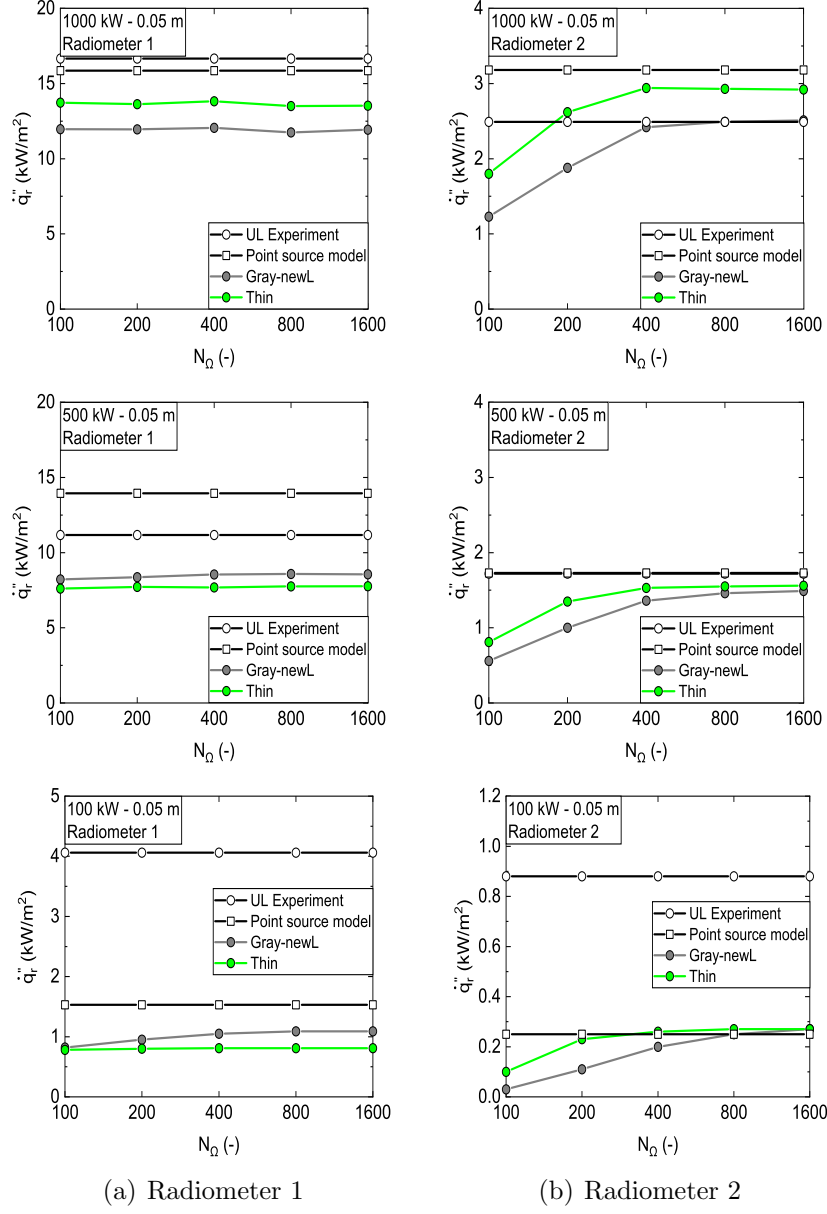(a) Radiometer 1   (b) Radiometer 2

Figure 9: Radiative heat fluxes with selected radiation modelling approaches with a 0.05 m grid size for different heat release rates and solid angles.

to be the best performing method, on average, compared to other simplified methods [44]. Nevertheless, the radiative heat flux predictions close to the fire with the point source model can have uncertainties given that near-field radiation is strongly influenced by the flame size, shape, and tilting, as well as the relative orientation of the target [45]. The CFD predictions, particularly at radiometer 1 (which is closest to the flame), are also closely linked to how accurately turbulence / combustion / radiation is modelled in the flame region, as well as on the CFD model settings (e.g., number of solid angles, discretization of the RTE, etc.). All these aspects could partially explain the differences observed in Figure 9.

6.5. Flame heights

Figure 10 presents the predicted flame heights with the 'Gray-newL' and 'Thin' radiation modelling approaches for different grid sizes and heat release rates. The predictions obtained with Heskestad's correlation (i.e., $L_f = 0.235\dot{Q}^{2/5} - 1.02D$) and the UL experimental data are also included for evaluation purposes of the simulations. The UL experimental data are close to Heskestad's correlation for the lower heat release case (i.e., 100 kW) but are systematically lower for the higher heat release rate cases (i.e., 500 kW and 1000 kW). Overall, the CFD predictions are in fairly good agreement with the experimental correlation if the flame heights are calculated based on the axial height where the integrated heat release rate is 99% of its total value for the 500 kW and 1000 kW cases. On the other hand, the numerical predictions for the 100 kW case are close to Heskestad's correlation if a threshold value of 95% is considered. This finding is perhaps not surprising as the 100 kW case is very close to the lower limit of the validity range of Heskestad's correlation. Overall, the flame heights are well predicted with the 'Gray-newL' model in most cases examined. It is worth noting that there were minor differences between the 'Gray-newL' and 'Gray' predictions in the numerical predictions (results not included here). On the other hand, the predictions with the 'Thin' model are consistently slightly lower compared to 'Gray-newL'. It is believed that this is a consequence of the emission occurring closer to the burner in the case of the 'Thin' model, which results in the integrated heat release rate to reach the prescribed threshold value faster (i.e., at axial location closer to the burner) compared to the 'Gray-newL' model.
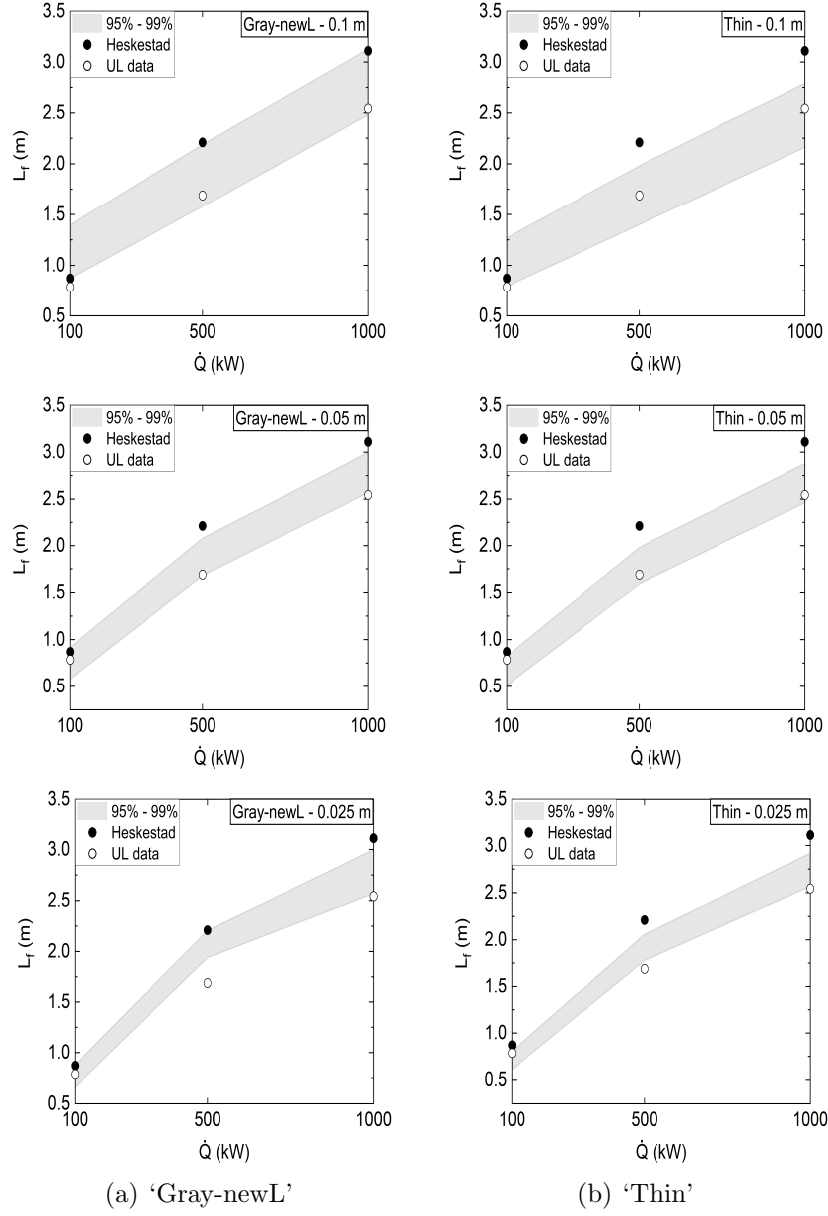
Figure 10: Flame heights (gray areas indicate an integrated HRR between 95-99%) using different radiation modelling approaches for different grid sizes and heat release rates.

6.6. Computational cost

Table 4 presents a brief overview of the computational cost associated with the different radiation models used in the study. To this purpose, the case with $\dot{Q} = 500$ kW, a 0.05 m grid size and 100 solid angles is chosen as a representative scenario. Nevertheless, similar findings were obtained for the rest of the scenarios as well. These are not reported here to avoid repetition. The default radiation model of FDS (i.e., 'Gray', 'Gray-newL)' is selected as the baseline case for comparison of the other approaches. The optically thin approach (i.e., 'Thin') is faster by approximately 9%, a finding which is expected because in this case no absorption coefficients need to be calculated during runtime. On the other hand, the 'WSGG' model is significantly more expensive, by approximately 240%: multiple RTEs need to be solved. In addition, increasing the number of solid angles, N_Ω, from 100 to 300 with the 'Gray' model, approximately doubled the required CPU time of the simulation.

Table 4: CPU cost between different radiation models for $\dot{Q} = 500$ kW and 0.05 m grid size using 18 MPI processors.

	CPU time (hour)*
Gray / Gray-newL	
$N_\Omega = 100$	427
$N_\Omega = 300$	897
Thin	
$N_\Omega = 100$	389
WSGG	
$N_\Omega = 100$	1447

* CPU time (hour) = Number of MPI processors $\times$ Wall time (hour).

7. Conclusions

The paper focused on examining the influence of the different radiation modelling approaches available in FDS (i.e., related to modelling of the absorption / emission term in the RTE) in scenarios involving under-resolved fires (i.e., typical for engineering-type of CFD simulations). Within this context, free-burn scenarios and well-established empirical correlations were

considered for validation of the numerical simulations. The different radiation modelling approaches that were tested involved the consideration of both an optically-thin ('Thin') and an optically-thick approach. In the latter case, the calculation of the local absorption coefficient was made with either the default gray gas model in FDS ('Gray'), the gray gas model but with a different path length L ('Gray-newL'), and a non-gray version of the Weighted Sum of Gray Gases model ('WSGG'). A simplified approach to estimate a priori the path length, L, in free-burn scenarios was reported.

As expected, the a priori estimation of the required spatial resolution based on the characteristic fire diameter (i.e., D^*) or the 'rule of thumb' (i.e., having at least 10 cells across the burner diameter) was shown to be sufficient for resolving the fire dynamics of the considered free-burn scenarios. There were some differences between the consideration of the optically-thin and the optically-thick approach available in FDS, particularly for the coarser grid size (0.1 m) and the highest HRR cases (500 kW, 1000 kW) considered, with the former (i.e., 'Thin') being more often closer to the experimental correlations available in the literature. The deviations in the predicted centerline axial velocities in the plume region with the latter approaches (i.e., 'Gray', 'Gray-newL') were up to 30% and 15% for the coarsest (0.1 m) and finest (0.025 m) grid size, respectively. In addition, the optically thick approaches exhibited a stronger grid sensitivity in the predicted radiative heat fluxes at locations close to the fire. The best predictions with the optically-thick approach were obtained with 'Gray-newL', however, increasing discrepancies were observed for all approaches with higher heat release rates. This was attributed to the under-prediction of the radiative fractions when trying to predict χ_r during the simulations (i.e., using the 'Gray', 'Gray-newL' or the 'WSGG' models). Overall, the calculation of the local absorption coefficient had an impact on the predicted values of the radiative fractions. The χ_r values were under-predicted by 11 - 20%, depending on the grid resolution, with the 'Gray' model. Changing the default value for the path length in FDS (i.e., from 10 cm to a higher value calculated based on the fire size - 'Gray-newL') only increased the predicted χ_r values by approximately 3 - 6%. On the other hand, the χ_r values were significantly under-predicted by the 'WSGG' model by more than 36%. The predicted χ_r values only increased by maximum 6 - 10% with decreasing grid size (i.e., from 0.1 m to 0.025 m) with the 'Gray' model, which confirms that the correction in the emission source term is necessary for obtaining accurate CFD predictions, particularly on relatively coarse grids. Any under-prediction of χ_r had

a noticeable impact on the predicted centerline temperature and axial velocity with increasing heat release rate with the effect, however, being less pronounced on the predicted radiative heat fluxes. The default number of solid angles in FDS (i.e., 100) was considered sufficient for targets that are relatively close to the burner but more solid angles were needed for targets positioned far away from the fire source. Nevertheless, the required number of solid angles will not only depend on the fire size but also on the distance between the fire source and the target of interest. Overall, even though FDS was able to capture fairly well the radiative emission from free-burn pool fires, there were some deficiencies in the predictions as well. These might, at least in part, be a natural consequence of the empirical nature of some of the employed models, in particular for turbulent combustion and radiation. The use of more fundamental and more advanced models could remedy these issues. Yet, these inherently come at a very (and often prohibitively) high computational cost for practical fire scenarios on the one hand, and they suffer from the limitation that in fires often the fuel is unknown a priori.

It is important to note that in the study at hand, the only source of radiation is the flame zone in the free fire plume (and to a much lesser extent the smoke plume). This is different from the configuration of a fire inside a compartment, where the location of the flame zone will depend on the configuration (including the ventilation openings), where there is usually a hot smoke layer and where the ceiling and walls participate in the radiation problem. These aspects will be further investigated in a future publication.

Acknowledgments

References

[1] McCaffrey, B.J., 1979. Purely Buoyant Diffusion Flames: Some Experimental Results. National Bureau of Standards, NBSIR 79-1910.

[2] Heskestad, G., 1998. Dynamics of the fire plume. Philos. trans. R. Soc. Lond. A 356, 2815-2833. https://doi.org/10.1098/rsta.1998.0299

[3] Klassen, M.E., Gore, J.P., 1994. Structure and radiation properties of pool fires. National Institute of Standards and Technology, NIST-GCR-94-651.

[4] McGrattan, K., Baum, H., Hamins, A., 2000. Thermal Radiation From Large Pool Fires. National Institute of Standards and Technology, NIS-TIR 6546. https://doi.org/10.6028/NIST.IR.6546

[5] Coelho, P.J., Teerling, O.J., Roekaerts, D., 2003. Spectral radiative effects and turbulence/radiation interaction in a non-luminous turbulent jet diffusion flame. Combust. Flame 133, 75-91. https://doi.org/10.1016/S0010-2180(02)00542-4

[6] Snegirev, A.Y., 2004. Statistical modeling of thermal radiation transfer in buoyant turbulent diffusion flames. Combust. Flame 136, 51-71. https://doi.org/10.1016/j.combustflame.2003.09.005

[7] Wang, L., Modest, M.F., Haworth, D.C., Turns, S.R., 2005. Modelling nongrey gas-phase and soot radiation in luminous turbulent nonpremixed jet flames. Combust. Theory Model. 9, 479-498. https://doi.org/10.1080/13647830500194834

[8] Wakatsuki, K., Jackson, G.S., Hamins, A., Nyden, M.R., 2007. Effects of fuel absorption on radiative heat transfer in methanol pool fires. Proc. Combustion Inst. 31, 2573-2580. https://doi.org/10.1016/j.proci.2006.08.049

[9] Consalvi, J.L., Demarco, R., Fuentes, A., Melis, S., Vantelon, J.P., 2013. On the modeling of radiative heat transfer in laboratory-scale pool fires. Fire Saf. J. 60, 73-81. https://doi.org/10.1016/j.firesaf.2012.10.010

[10] Consalvi, J.L., Liu, F., 2014. Radiative heat transfer in the core of axisymmetric pool fires – I: Evaluation of approximate radiative property models. Int. J. Therm. Sci. 84, 104-117. https://doi.org/10.1016/j.ijthermalsci.2014.04.018

[11] Xu, R., Le, V.M., Marchand, A., Verma, S., Rogaume, T., Richard, F., Luche, J, Trouvé, A., 2021. Simulations of the

coupling between combustion and radiation in a turbulent line fire using an unsteady flamelet model. Fire Saf. J. 120, 103101. https://doi.org/10.1016/j.firesaf.2020.103101

[12] Merci, B., Li, J., Maragkos, G., 2023. On the importance of the heat release rate in numerical simulations of fires in mechanically ventilated air-tight enclosures, Proc. Combustion Inst. 39, 3647-3672. https://doi.org/10.1016/j.proci.2022.06.011

[13] Ahmed, M.M., Trouvé, A., 2021. Large eddy simulation of the unstable flame structure and gas-to-liquid thermal feedback in a medium-scale methanol pool fire. Combust. Flame 225, 237-254. https://doi.org/10.1016/j.combustflame.2020.10.055

[14] Koseki, H., Yumoto, T., 1988. Air entrainment and thermal radiation from heptane pool fires. Fire Technol. 24, 33-47. https://doi.org/10.1007/BF01039639

[15] McGrattan, K., Floyd, J., Forney, G., Baum, H., Hostikka, S., 2003. Improved Radiation and Combustion Routines for a Large Eddy Simulation Fire Model. Fire Saf. Sci. 7, 827-838. http://dx.doi.org/10.3801/IAFSS.FSS.7-827

[16] McGrattan, K., Hostikka, S., Floyd, J., McDermott, R., Vanella, M., 2022. Fire Dynamics Simulator User's Guide. National Bureau of Standards, NIST Special Publication 1019, Sixth Edition.

[17] McGrattan, K., Hostikka, S., Floyd, J., McDermott, R., Vanella, M., 2022. Fire Dynamics Simulator Technical Reference Guide Volume 1: Mathematical Model. National Institute of Standards and Technology, NIST Special Publication 1018-1, Sixth Edition.

[18] Deardorff, J.W., 1980. Stratocumulus-capped mixed layers derived from a three-dimensional model. Bound. -Layer Meteorol. 18, 495-527. https://doi.org/10.1007/BF00119502

[19] Pope, S.B. , 2000. Turbulent Flows, 1st edition. Cambridge University Press, Cambridge. https://doi.org/10.1017/CBO9780511840531

[20] Magnussen, B.F., Hjertager, B.H., 1977. On mathematical modeling of turbulent combustion with special emphasis on soot

formation and combustion. Symp. (Int.) Combust. 16, 719-729. https://doi.org/10.1016/S0082-0784(77)80366-4

[21] McDermott, R., McGrattan, K., Floyd, J., 2011. A Simple Reaction Time Scale for Under-Resolved Fire Dynamics. Fire Saf. Sci. 10, 809-820. 10.3801/IAFSS.FSS.10-809

[22] Heskestad, G., 1984. Engineering relations for fire plumes. Fire Saf. J. 7, 25-32. https://doi.org/10.1016/0379-7112(84)90005-5

[23] Siegel, R., Howell, J.R., 1981. Thermal Radiation Heat Transfer,, 2nd edition. Hemisphere Publishing Corporation, New York, Cambridge.

[24] Grosshandler, W., 1993. RadCal: A Narrow Band Model for Radiation Calculations in a Combustion Environment. NIST Technical Note 1402, National Institute of Standards and Technology. https://doi.org/10.6028/NIST.TN.1402

[25] Hottel, H.C., Sarofim, A.F., 1967. Radiative Transfer, 1st edition. McGraw-Hill, New York. https://doi.org/10.1002/aic.690150504

[26] Krishnamoorthy, G., 2010. A comparison of gray and non-gray modeling approaches to radiative transfer in pool fire simulations. J. Hazard. Mater. 182, 570-580. http://dx.doi.org/10.1016/j.jhazmat.2010.06.071

[27] Sikic, I., 2018. Radiative heat transfer for modelling fire and fire suppression. PhD thesis, University of Warwick.

[28] Fraga, G.C., Silva, F.R., Zanin, L.G.B., da Fonseca, R.J.C., França, F.H.R., Centeno, F.R., 2021. A comprehensive evaluation of the WSGG model for air- and oxy-fuel combustion conditions through three-dimensional calculations. Fire Saf. J. 125, 103433. https://doi.org/10.1016/j.firesaf.2021.103433

[29] Bordbar, M.H., Wecel, G., Hyppanen, T., 2014. A line by line based weighted sum of gray gases model for inhomogeneous CO2-H2O mixture in oxy-fired combustion. Combust. Flame 161, 2435-2445. https://doi.org/10.1016/j.combustflame.2014.03.013

[30] Chungen, Y., Johansen, L.C.R., Rosendahl, L.A., Kær, S.K., 2010. New Weighted Sum of Gray Gases Model Applicable to Computational

Fluid Dynamics (CFD) Modeling of Oxy-Fuel Combustion: Derivation, Validation, and Implementation. Energy Fuels 24, 6275-6282. https://doi.org/10.1021/ef101211p

[31] Peters, N., 1984. Laminar diffusion flamelet models in non-premixed turbulent combustion. Prog. Energy Combust. Sci. 10, 319-339. https://doi.org/10.1016/0360-1285(84)90114-X

[32] Klimenko, A.Y., Bilger, R.W., 1999. Conditional moment closure for turbulent combustion. Prog. Energy Combust. Sci. 25, 595-687. https://doi.org/10.1016/S0360-1285(99)00006-4

[33] Kruljevic, B., 2021. Fundamental study in applications of the conditional moment closure method to fire-related flows. PhD thesis, Ghent University, Belgium.

[34] Pope, S.B., 1985. PDF methods for turbulent reactive flows. Prog. Energy Combust. Sci. 11, 119-192. https://doi.org/10.1016/0360-1285(85)90002-4

[35] Ren, T., Modest, M.F., Haworth, D.C., 2018. Simulating turbulence–radiation interactions using a presumed probability density function method. Int. J. Heat Mass Transf. 121, 911-923. https://doi.org/10.1016/j.ijheatmasstransfer.2018.01.049

[36] McGrattan, K., Hostikka, S., Floyd, J., McDermott, R., Vanella, M., 2022. Fire Dynamics Simulator Technical Reference Guide Volume 3: Validation. National Institute of Standards and Technology, NIST Special Publication 1018-3, Sixth Edition.

[37] Bordbar, H., Hostikka, S., Boulet, P., Parent, G., 2020. Numerically resolved line by line radiation spectrum of large kerosene pool fires. J. Quant. Spectrosc. Radiat. Transf. 254, 107229. doi:10.1016/j.jqsrt.2020.107229

[38] Fernandes, C.S., Fraga, G.C., França, F.H.R., Centeno, F.R., 2021. Radiative transfer calculations in fire simulations: An assessment of different gray gas models using the software FDS. Fire Saf. J. 120, 103103. https://doi.org/10.1016/j.firesaf.2020.103103

[39] Alinejad, F., Bordbar, H., Hostikka, S., 2020. Development of full spectrum correlated k-model for spectral radiation penetration within liquid fuels. Int. J. Heat Mass Transf. 158, 119990. https://doi.org/10.1016/j.ijheatmasstransfer.2020.119990

[40] Consalvi, J.L., Andre, F., Coelho, F.R., Franca, F.H.R., Nmira, F., Galtier, M., Solovjov, V., Webb, B.W., 2020. Assessment of engineering gas radiative property models in high pressure turbulent jet diffusion flames. J. Quant. Spectrosc. Radiat. Transf. 253, 107169. https://doi.org/10.1016/j.jqsrt.2020.107169

[41] McKinnon, M., Willi, J., Madrzykowski, D., 2021. Examination of Fire Dynamics Analysis Techniques: Assessment of Predictive Fire Algorithms and Models. Underwriters Laboratories Report, UL Firefighter Safety Research Institute.

[42] Modak, A.T., 1977. Thermal radiation from pool fires. Combust. Flame 29, 177-192. https://doi.org/10.1016/0010-2180(77)90106-7

[43] Beyler, C., 2016. Chapter 66 - Fire Hazard Calculations for Large, Open Hydrocarbon Fires. in: SFPE Handbook of Fire Protection Engineering, Springer.

[44] Fleury, R., 2011. Evaluation of Thermal Radiation Models for Fire Spread between Objects. PhD thesis, University of Canterbury.

[45] N. Iqbal, M.H. Salley, Fire Dynamics Tools (FDTs): Quantitative Fire Hazard Analysis Methods for the U.S. Nuclear Regulatory Commission Fire Protection Inspection Program, Washington, DC: U.S. Nuclear Regulatory Commission, 2004.